Pesquisas em Geociências, v. 46 (2019), n. 1: e0734 E-ISSN 1807-9806
Instituto de Geociências, Universidade Federal do Rio Grande do Sul, Porto Alegre, RS, Brasil doi.org/10.22456/1807-9806.93249

Structural control of REE-pegmatites associated with the world-class Sn-Nb-Ta-cryolite deposit at the Pitinga mine, Amazonas, Brazil

Fernanda Claas RONCHI[1], Fernando Jacques ALTHOFF[2], Artur Cezar BASTOS NETO[1,3] & Harald G. DILL[4]

[1] Programa de Pós-graduação em Geociências, Universidade Federal do Rio Grande do Sul. Av. Bento Gonçalves, 9.500, CEP 91540-000, Porto Alegre, RS, Brasil (fcronchi@gmail.com, artur.bastos@ufrgs.br).

[2] Departamento de Geologia, Centro de Filosofia e Ciências Humanas, Universidade Federal de Santa Catarina. Campus Universitário, Trindade, CEP 88040-970, Florianópolis, SC, Brasil (althoff@cfh.ufsc.br).

[3] Programa de Pós-graduação em Avaliação de Impactos Ambientais, Universidade La Salle. Av. Victor Barreto, 2288, CEP 92010-000, Canoas, RS, Brasil.

[4] Gottfried Wilhelm Leibniz Universität, Welfengarten 1 D-30167 Hannover, Germany (haralddill@web.de).

Abstract. We have studied the structural control of pegmatites (F-REE-Li vein-type granite pegmatite) associated with the albite-enriched granite facies (AEG) of the Madeira A-type granite (~1.83 Ga). This facies corresponds to the Madeira world-class Sn-Nb-Ta-F (cryolite) deposit at the Pitinga mine. These REE-rich pegmatites [xenotime-(Y) and gagarinite-(Y)], presently exploited together with the disseminated ore, have potential to exploitation by selective mining. They have a common geometric arrangement and share the same mineralogy, therefore they all originated from the same source. They have the same mineralogical composition of the host rock and their emplacement occurred in the parental rock itself. The geometric arrangement of the pegmatites is settled by contractional brittle structures (reverse faults, imbrication fans and horses). The reverse fault planes (~N320/60SW) were essentially the conduits for the fluid. The preferential sites for the pegmatites bodies were horizontal tensile fractures. The well-marked geometric arrangement of the tectonic structures and the fact that there are also reverse faults planes without pegmatites show that the fractures that host the pegmatites were not formed by the fluid pressure. The orientation of the contractional structures in the AEG indicates a transport from SW to NE. With reduced dimensions, the AEG cooled fast, however its location in the cold upper crust and the low *solidus* temperature allowed pegmatites formation. The pegmatites were formed with the AEG emplaced in a structural level above the critical crustal depth, where minimum normal stress is vertical.

Keywords. pegmatite, structural control, albite-enriched granite, rare earth elements, Pitinga mine, Amazonas.

Resumo. Controle estrutural dos pegmatitos ricos em ETR associados ao depósito Madeira (Sn-Nb-Ta), mina Pitinga, Amazonas, Brasil. Estudou-se o controle estrutural dos veios de pegmatitos graníticos (tipo F-ETR-Li) associados à fácies albita granito (AEG) do granito Madeira (~1.83Ga). Esta fácies corresponde ao depósito, de classe mundial de Sn-Nb-Ta-F (criolita) da mina de Pitinga. Atualmente, esses pegmatitos ricos em ETR [xenotima-(Y) e gagarinita-(Y)] são explorados junto com o minério disseminado, porém possuem potencial para exploração por lavra seletiva. Todos os pegmatitos se enquadram em um mesmo arranjo geométrico e apresentam uma mesma mineralogia, o que sugere que se originaram de uma mesma fonte. Sua mineralogia é igual à da encaixante, o que sugere que seu alojamento ocorreu na própria rocha parental. O arranjo geométrico dos pegmatitos é determinado por estruturas contracionais frágeis (falhas inversas, leques imbricados e cavalos). Os planos de falhas inversas (N320/60SW) serviram como condutos para o fluido que se alojou preferencialmente em fraturas horizontais distensivas. O arranjo geométrico bem definido dessas estruturas e o fato de que também há planos de falhas inversas sem pegmatitos sugerem que as fraturas que hospedam os pegmatitos não foram geradas pela pressão do fluido. A orientação das estruturas contracionais no AEG indica que ocorreu um transporte de SW para NE. Como este corpo possui pequena dimensão, resfriou-se rapidamente. Contudo, sua localização na crosta superior fria e a baixa temperatura do solidus permitiram a formação dos pegmatitos. Os pegmatitos foram formados com o AEG colocado em um nível estrutural acima da profundidade crustal crítica, onde a tensão mínima normal é vertical.

Palavras-chave. pegmatito, controle estrutural, albita granito, elementos terras raras, Pitinga, Amazonas.

1 Introduction

As reflected in classification schemes and contents of reviews papers, the studies of granitic pegmatites are based mostly on textural, geochemical and isotopic characteristics and on the geotectonic setting of granite magmatism. Data about the structural relationship of the pegmatites with the host rocks, that interact to control size, shape and orientation of pegmatite bodies, are still rare. However, the understanding of the structural elements of the host rock is necessary in the study of pegmatite bodies emplaced at upper levels in the crust (Dill, 2016, 2018). There is a lack of structural data concerning pegmatites because studies are generally focused on the processes responsible for the formation of the remarkable characteristics of pegmatites, and not on the study of the pegmatites as rock bodies. The structural analysis of pegmatite bodies can provide not only information about the controls of the mineralization processes during the final stages of the magmatic activity, but also about changes in the tectonic setting through the time of intrusion to the late stage hypogene alteration.

This work is focused in the structural analysis of pegmatite bodies associated with the albite-enriched granite facies (AEG) of the Madeira A-type granite (~1.83 Ga), in the Pitinga mine, located in the Amazonian craton, northern Brazil. The AEG corresponds to the Madeira world-class Sn-Nb-Ta (REE, Zr, U, Th, cryolite) deposit. This association of cryolite, Sn, Nb and Ta and several other rare metals disseminated in the same peralkaline rock which also hosts a massive cryolite deposit is unique in the world. At present, the pegmatites are explored together with the disseminated Sn-Nb-Ta ore. However, since they are rich in xenotime-(Y), particularly rich in Dy, and also contain gagarinite-(Y), their exploitation through selective mining is being evaluated.

2 Geological setting and methods

2.1 Geological setting

The Pitinga region is situated near to the Equator line, in the southern part of the Guyana shield (Gibbs & Barron, 1983). Geophysical surveys (Rosa et al., 2014) were instrumental in the localization of the Pitinga region (Fig. 1A) in the Central Amazonian Province (> 2.3 Ga), at the edge with the Ventuari-Tapajós Province (1.95 to 1.8 Ga) of the Amazonian craton (Tassinari & Macambira, 1999).

The Madeira granite composes the Madeira Suite with the Europa and Água Boa granites (Costi, 2000). It is emplaced in volcanic rocks of the Iricoumé Group (1881 ± 2 to 1890 ± 2 Ma, ^{207}Pb-^{206}Pb in zircon; Ferron *et al.,* 2006). Four facies are characterized in the Madeira granite (Fig. 1B). The oldest is an amphibole-biotite syenogranite (1824 ± 2 Ma, Pb-Pb in zircon; Costi, 2000). This facies is cross cut by a biotite-alkali feldspar granite (1822 ± 2 Ma, Pb-Pb in zircon; Costi, 2000) and subsequently by an alkali feldspar *hypersolvus* porphyritic granite (1818 ± 2Ma, Pb-Pb in zircon; Costi, 2000). The AEG, which has very methamitic zircons (1822 ± 22 Ma, U-Pb in zircon; Bastos Neto *et al*., 2014), exhibits magma-mingling relationship with the *hypersolvus* granite facies. The AEG is the unique mineralized facies and host the pegmatites studied in this paper.

The AEG has an ellipsoidal shape with the N-S axis measuring 2 km and the E-W 1.5 km. It is divided into core albite-enriched granite (CAG) and border albite-enriched granite (BAG) (Fig. 2). The CAG is a subsolvus granite, porphyritic to seriate in texture, fine to medium in grain size, and composed of quartz, albite, and K-feldspar in nearly equal proportions (25 to 30%). The accessory minerals are cryolite (5%), polylithionite (4%), biotite (3%), zircon (2%), and riebeckite (2%). Pyrochlore, cassiterite, xenotime-(Y), columbite, thorite, magnetite, genthelvite and galena occur in minor proportions. The BAG is a peraluminous granite with the same texture types and essential mineralogy as the CAG core, except for iron-rich minerals, which have almost completely disappeared because of an autometasomatic process, and the presence of fluorite instead of cryolite (Costi *et al.*, 2000; 2009). The disseminated ore (CAG + BAG) totalizes 164 Mt with 0.17 wt.% Sn, 0.22 wt.% Nb_2O_5 and 0.028 wt.% Ta_2O_5.

In the central portion of CAG, in depth not yet reached by the mining operations, occurs a

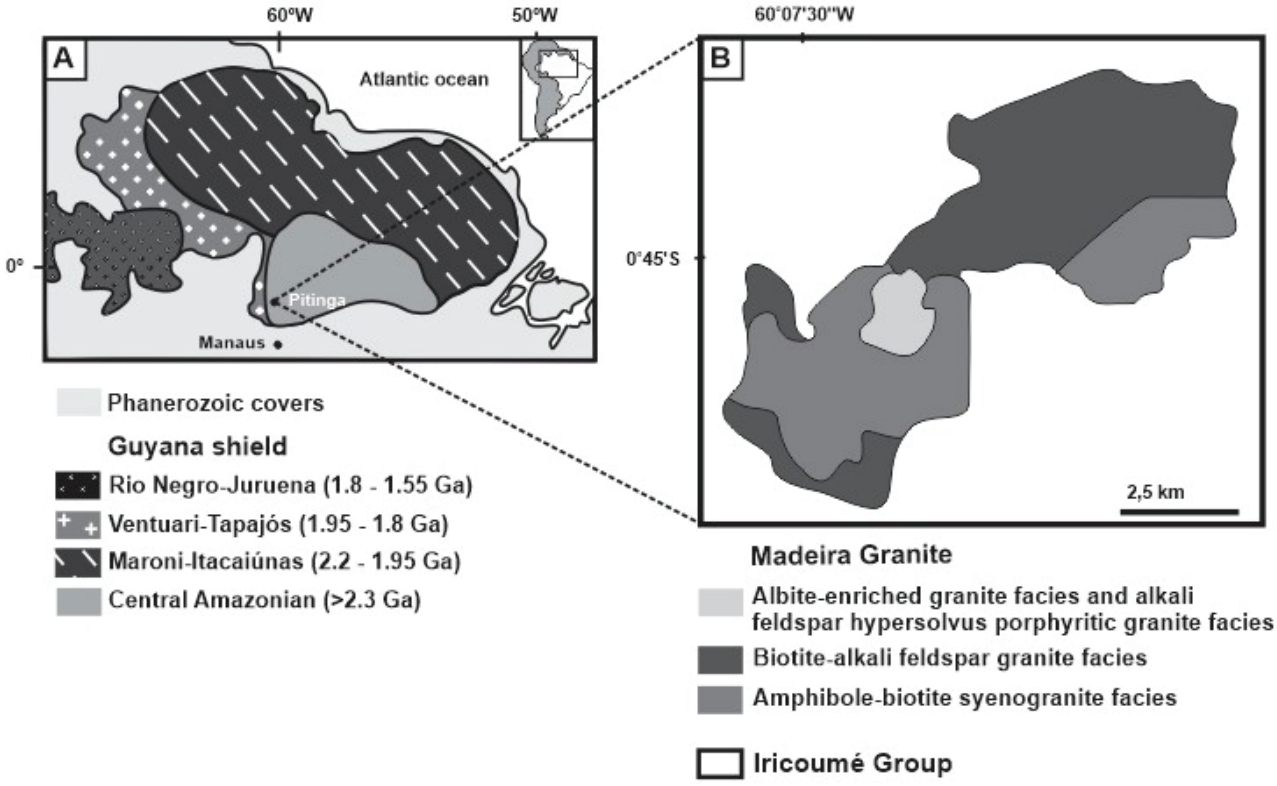

Figure 1. Geological setting and location of Pitinga region. A) Geochronological provinces of the Amazonian craton in the Guyana shield (modified from Tassinari & Macambira, 1999); B) Geological map of the Madeira granite (after Costi, 2000).
Figura 1. Configuração geológica e localização da região de Pitinga. A) Províncias geocronológicas do Cráton Amazônico no escudo das Guianas (modificado de Tassinari & Macambira, 1999); B) Mapa geológico do granito Madeira (segundo Costi, 2000).

massive cryolite deposit of 10 Mt with a grade of 31.9 wt.% Na_3AlF_6. This deposit is formed by several massive bodies of cryolite that are intercalated with the CAG and *hypersolvus* granite. These cryolite bodies are subhorizontal, can be up to 300 m long and 30 m thick, and are made up essentially of cryolite crystals (approximately 87% by volume), plus quartz, zircon, and feldspar. Bastos Neto *et al.* (2005, 2009) and Minuzzi *et al.* (2006) provided detailed descriptions.

Several authors (e.g. Costi, 2000; Minuzzi *et al*., 2006; Pires, 2010; Bastos Neto *et al*., 2014) reported the existence of pegmatites associated to the CAG. Pires (2010) highlighted the abundance of the pegmatites in xenotime-(Y) and their potential to explotation by selective mining. All the minerals of the CAG listed above occur in the pegmatite veins. Quartz, feldspar, cryolite, polylithionite, and riebeckite are commonly well-developed (Fig. 3A), often-reaching 5 cm, locally 10 cm or more. Xenotime-(Y) is not so developed, the larger crystals are in the order of 2 cm, but crystals such as these may be very abundant (Fig. 3B). In the CAG also occurs the pegmatitic AEG (Bastos Neto *et al*., 2009; Stolnik, 2015), a textural variation of the AEG in the form of bands or lenses, with gradational contact, mineralogy similar to AEG, but with very coarse texture. The pegmatitic AEG is not subject of this paper, that focused in the pegmatite veins.

The maximum temperature estimated for the beginning of the crystallization of the amphibole-biotite sienogranite (the oldest facies) is 930 °C, at a depth of approximately 15 km (5 kbar) and, for the AEG, is below 650 °C at depth of approximately 1km (1 kbar) (Lenharo *et al*., 2003). According to Lenharo (1998) and Costi (2000), there would have been an extreme F-enrichment in the residual melt of the AEG, responsible for the formation of the massive cryolite deposit. This deposit would be related to a silicate-fluoride liquid-liquid immiscibility (Lenharo's model) or to the melt split into a high-water, relatively F-poor portion, and a low-water, Na-Al-F-rich residual portion (Costi's model). However, according to Bastos Neto *et al*. (2009),

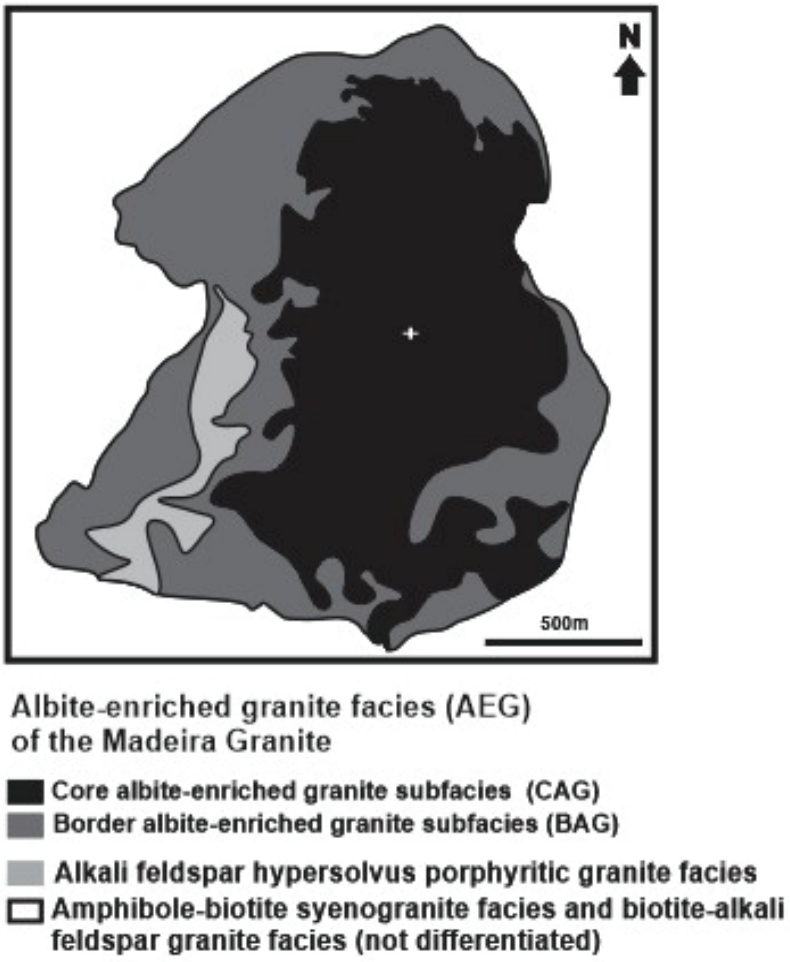

Figure 2. Geological map of the albite-enriched granite (after Minuzzi et al., 2006). The crosses in figures 2 and 4 indicate the same point.
Figura 2. Mapa geológico do albita granito (segundo Minuzzi et al., 2006). As cruzes nas figuras 2 e 4 indicam o mesmo ponto.

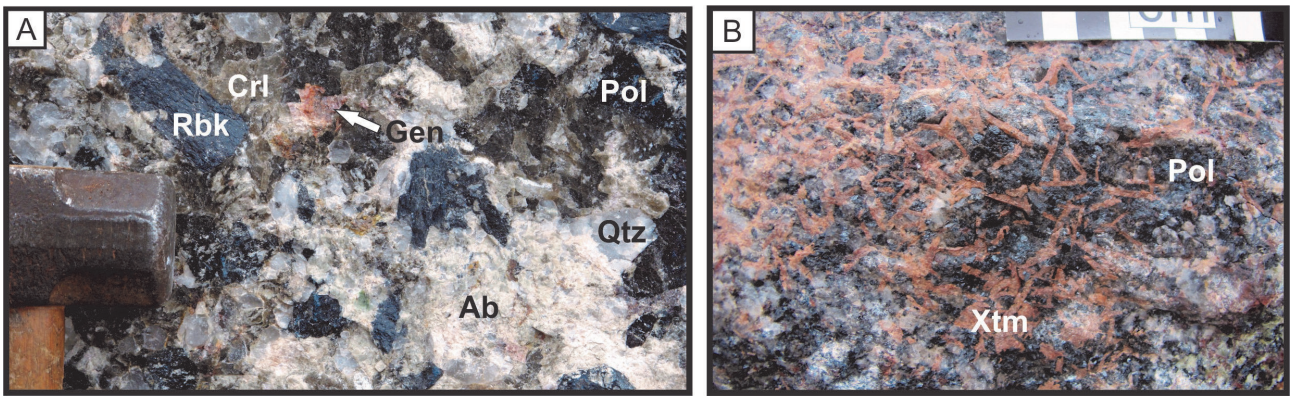

Figure 3. Minerals of pegmatites. A) Pegmatite vein formed by albite (Ab), quartz (Qtz), riebeckite (Rbk), polylithionite (Pol), cryolite (Crl), and genthelvite (Gen); B) Pegmatite rich in xenotime-(Y) (Xtm) and polylithionite (Pol).
Figura 3. Minerais dos pegmatitos. A) Veio de pegmatito formado por albita (Ab), quartzo (Qtz), riebeckita (Rbk), polilitionita (Pol), criolita (Crl) e genthelvita (Gen); B) Pegmatito rico em xenotima-(Y) (Xtm) e polilitionita (Pol).

the extreme F-enrichment did not occur because the crystallization of magmatic cryolite since the earlier stages buffered the content of F in the melt. In addition, the fluid inclusions data proved that the massive cryolite deposit is hydrothermal, formed from an aqueous fluid (salinity ranges from 1.7 to 22.4 wt.% eq. NaCl). The highest homogenization temperature measured in massive cryolite is 400 °C; the cryolite formation continued until ~100 °C.

2.2 Methods

Detailed structural analysis was carried out in the open pit of the Pitinga mine, in the benches between levels 210 and 140 (Fig. 4). The main tectonic structures were characterized and their geometric relationships investigated. Microstructural analysis in standard thin sections of the host rock and pegmatite minerals was made with the objective of determining whether or not they were affected by tectonic deformation. The description of contractional structures employs the terminology of Boyer & Elliott (1982). The term pegmatite *vein* is used in the sense of Bons *et al*. (2012): "aggregate of minerals precipitated from a fluid at a dilatation site".

3 Results

3.1 Structural geology of the CAG

In the current exposed surface of the CAG occurs principally reverse faults, imbrication fans and horses (Fig. 5A). The reverse faults occur as single slip surface or as composing fault zones. Even the fault zones have core and damage zones with centimeter thick, that suggest small

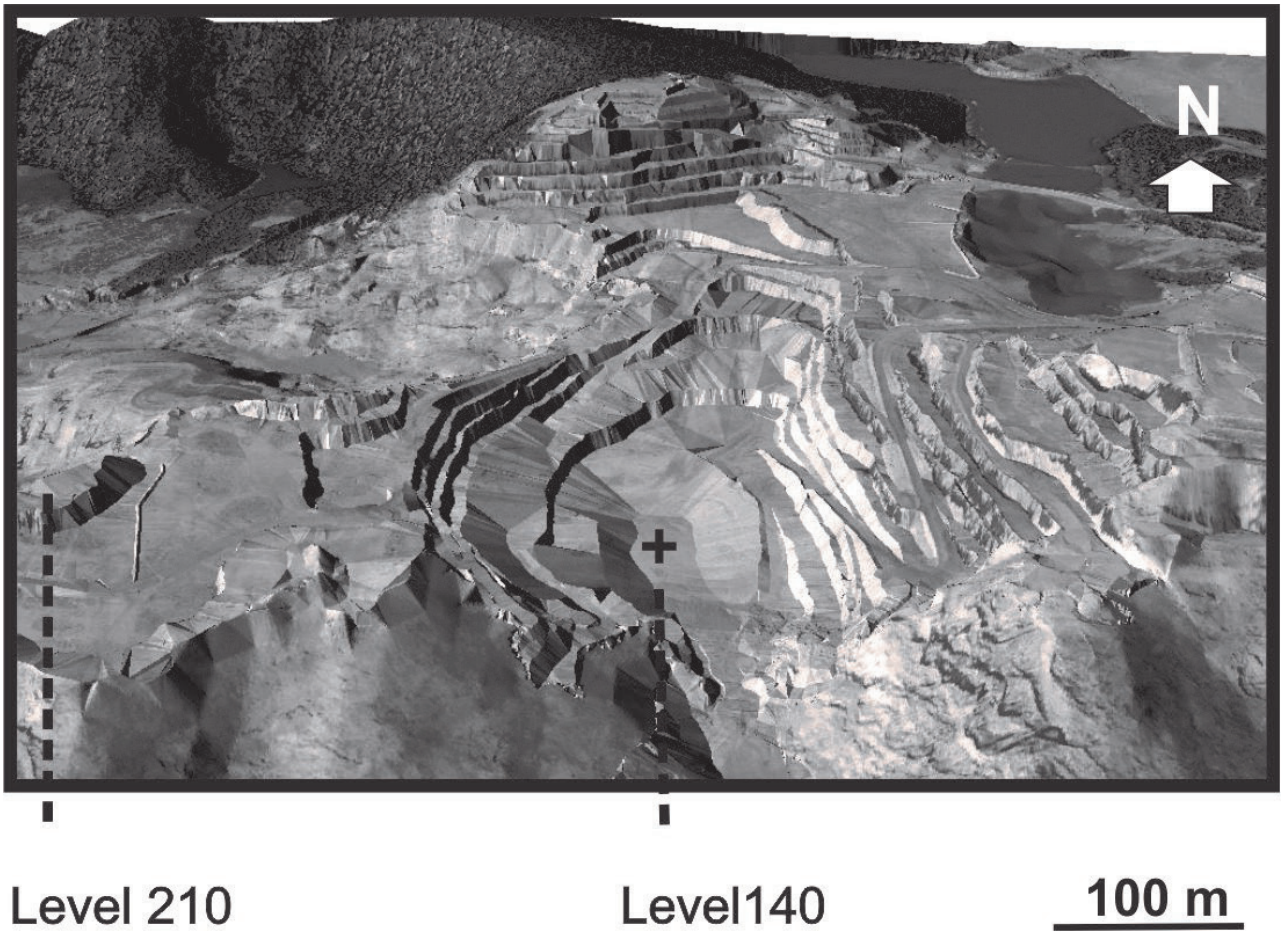

Figure 4. Pitinga mine open pit 3D model (october 2016). The crosses in figures 4 and 2 are located in the same point. Provided by Mineração Taboca Ltda.
Figura 4. Modelo 3D da lavra a céu aberto na mina Pitinga (outubro de 2016). As cruzes nas figuras 4 e 2 indicam o mesmo ponto. Fornecido pela Mineração Taboca Ltda.

slips. Despite the small thickness, the faults are penetrative and one same fault may be tracked through several levels benches. The fault planes are oriented N300 to 340, with dips between 45^0 and 80^0 predominantly to SW. Reverse fault planes with dips to NE are less common. Some sigmoidal fault planes delimit horses with meter to centimeter scales, with S geometry and dip to SW (Fig. 5B). The imbrication fans have meter to decameter sizes, with thrust transport to NE. In the structures of this set, the fault-slip direction is perpendicular to the strike of fault planes, as recorded by slickenlines and chatter marks (Fig. 5C). The prevalence of reverse fault planes with dips to SW strongly suggests that transport was predominantly to NE.

A widespread network of horizontal extension fractures is associated to the reverse faults. These fractures have meter length and millimeter to centimeter width, when they are not filled (Fig. 6). The intersection of NE and SW dip fault planes create convex linear features with orientation around N330, which sometimes are prominent in the benches (Fig. 7A, B). The geometric array of the contractional structures of the AEG (visibles in the CAG) is summarized in

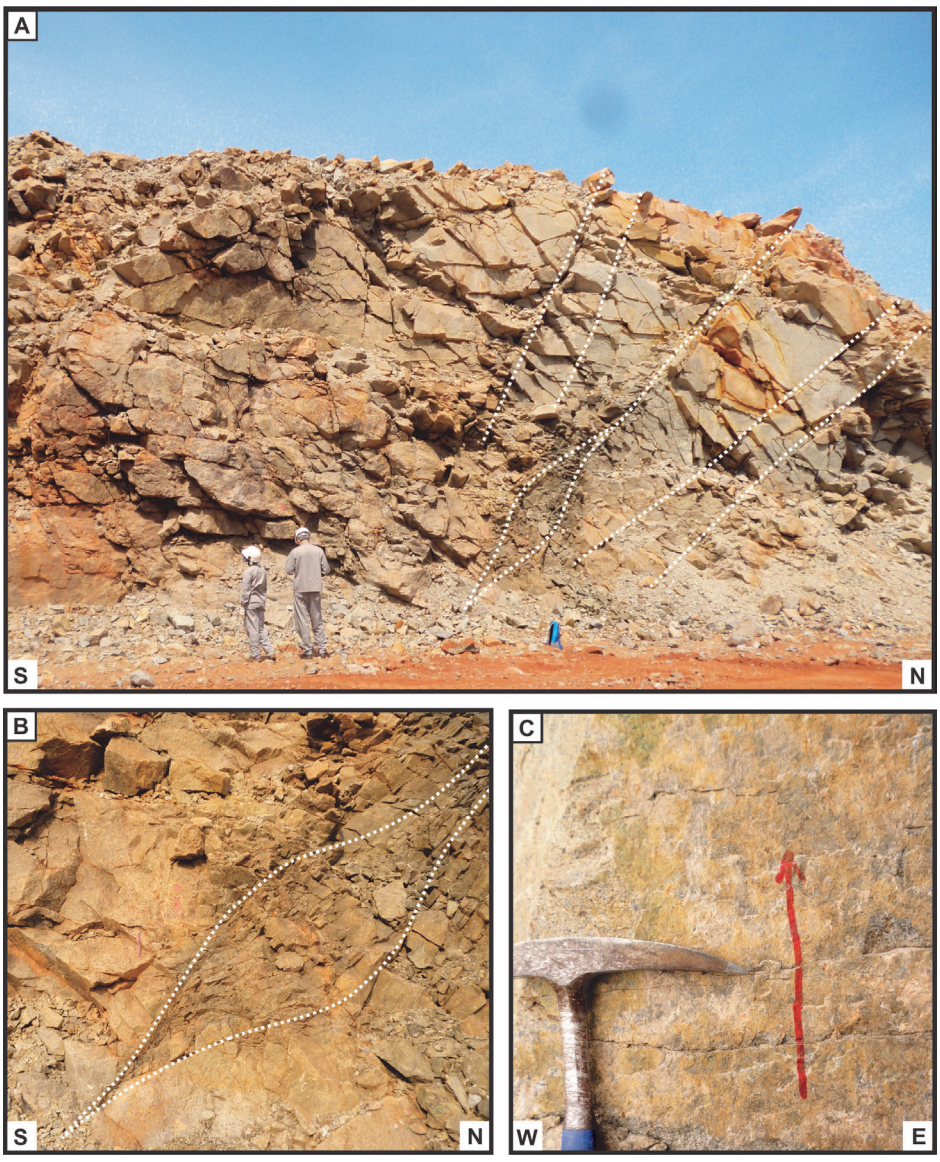

Figure 5. Tectonic structures in the CAG. A) Imbrication fan with horse in the core albite-enriched granite. Reverse faults N300/45-60SW; B) Detail of the meter horse observed in A (photo width: 2m); C) Chatter marks in reverse fault plane in the CAG. The missing block moved up.
Figura 5. Estruturas tectônicas no CAG. A) Leque imbricado com cavalo no albita granito de núcleo. Planos de falhas inversas N300/46-60SW; B) Detalhe de um cavalo métrico observado em A (largura da foto: 2m); C) Chatter marks em plano de falha inversa no CAG. O bloco ausente subiu.

the stereogram of the Fig. 8A. It may be related to a stress field in wich σ1= 10/230, σ2= 0/320 and σ3= 80/050 (Fig. 8B). The extension fractures are parallels to, or contain, the maximum (σ1) and the intermediate (σ2) principal stresses and are perpendicular to the minimum stress (σ3). As will be shown below, the contractional structures control the orientation of the pegmatite bodies.

Less commons structures are very low angle reverse faults with main orientation around N20E and dip < 20° to NW or SE. The fault planes are filled with riebeckite or cryolite. Slickenlines indicate transport from ESE to WNW (Fig. 9A). In addition, there are hybrid fractures (N310/75SW) filled with fibrous cryolite (15/N213) (Fig. 9B). The orientations of both groups of structures are consistent with a stress field where σ1= 0/300 and σ3= 15/210 (Fig. 10).

The orientations of the two sets of structures observed in the open pit are not in agreement with a same principal stress axes orientation. This suggests that the formation of cryolite may have been asynchronous with the emplacement of the pegmatite bodies.

3.2 Pegmatite veins

In the open pit pegmatites are observed in miarolitic cavities and veins. The miarolitic cavities are not ubiquitous. They have centimeter to decimeter sizes and are filled with quartz, chlorite, fluorite and cryolite (Bastos Neto *et al*., 2014). These pegmatite bodies are not associated with fractures (Fig. 11A). They seem to occur more closer to the CAG - BAG boundary. In some miarolitic cavities a well-marked zonation is observed. The thickness of the border zone is centimetric; it is formed by quartz and albite

Figure 6. Horizontal extension fractures (dotted black lines) associate to reverse faults (continuous black lines). Doble arrows indicate the opening direction of horizontal fractures.
Figura 6. Fraturas extensionais horizontais (linhas tracejadas pretas) associadas a falhas inversas (linhas contínuas pretas). Setas duplas indicam o sentido de abertura das fraturas horizontais.

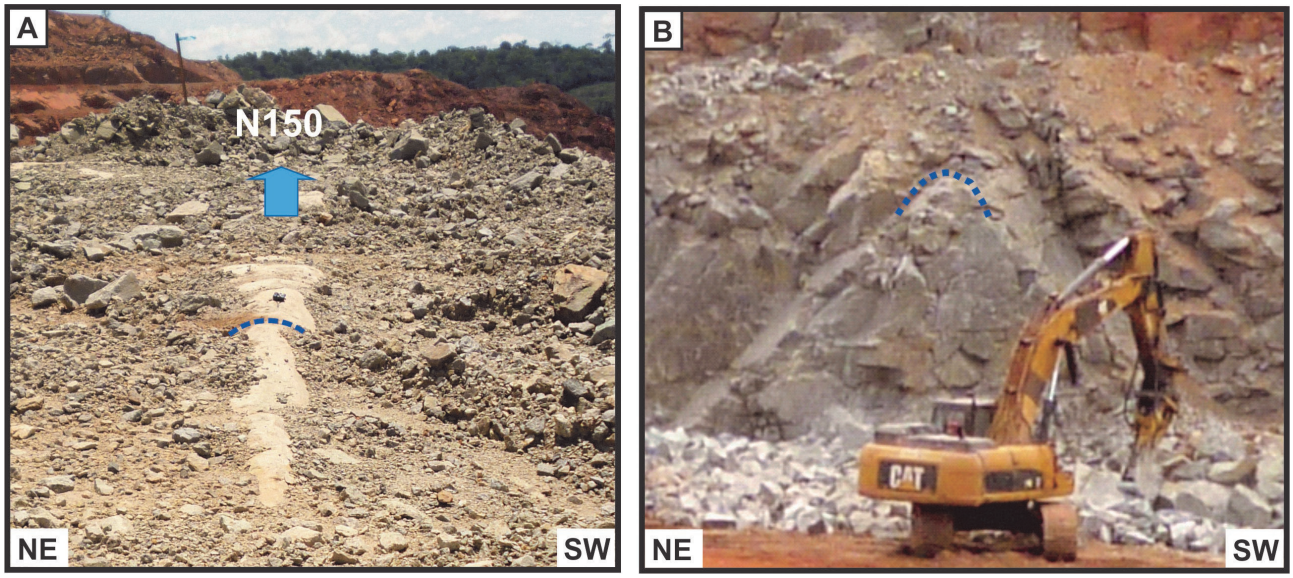

Figure 7. Linear structure formed by the intersection of the reverse fault planes dipping down NE and SW. A) Plane view; B) Section view.
Figura 7. Estrutura linear formada pela intersecção dos planos de falhas inversas mergulhando para NE e SW. A) Vista em plano; B) Vista em perfil.

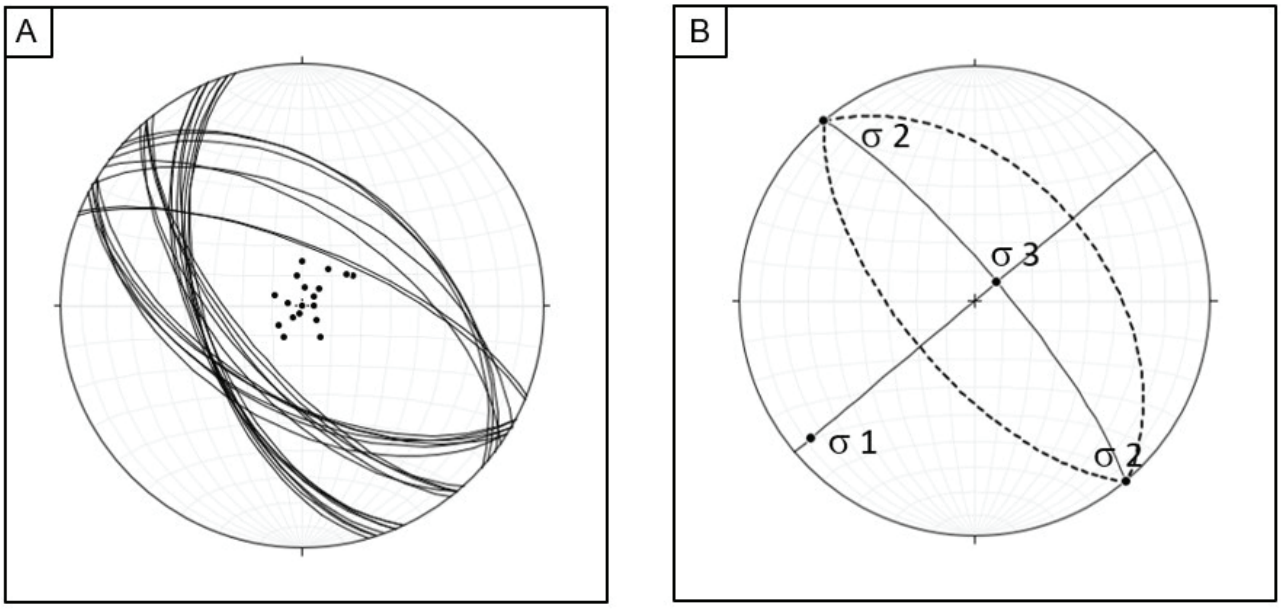

Figure 8. Stereogram with the geometric array of the contractional structures of the CAG. A) Reverse fault planes (great circles) and poles of extension fractures (dots) in the core albite-enriched granite (N: 56); B) Orientation of the principal stress axes related to the contractional structures of the CAG. Equal-area (Schmidt-Lambert) stereographic projection, lower hemisphere.
Figura 8. Estereograma com o arranjo geométrico das estruturas contracionais do CAG. A) Planos de falhas inversas (grandes círculos) e polos das fraturas extensionais (pontos) no albita granito de núcleo (N: 56); B) Orientação dos eixos principais de esforços relacionados às estruturas contracionais do CAG. Projeção estereográfica equiárea (Schmidt-Lambert) hemisfério inferior.

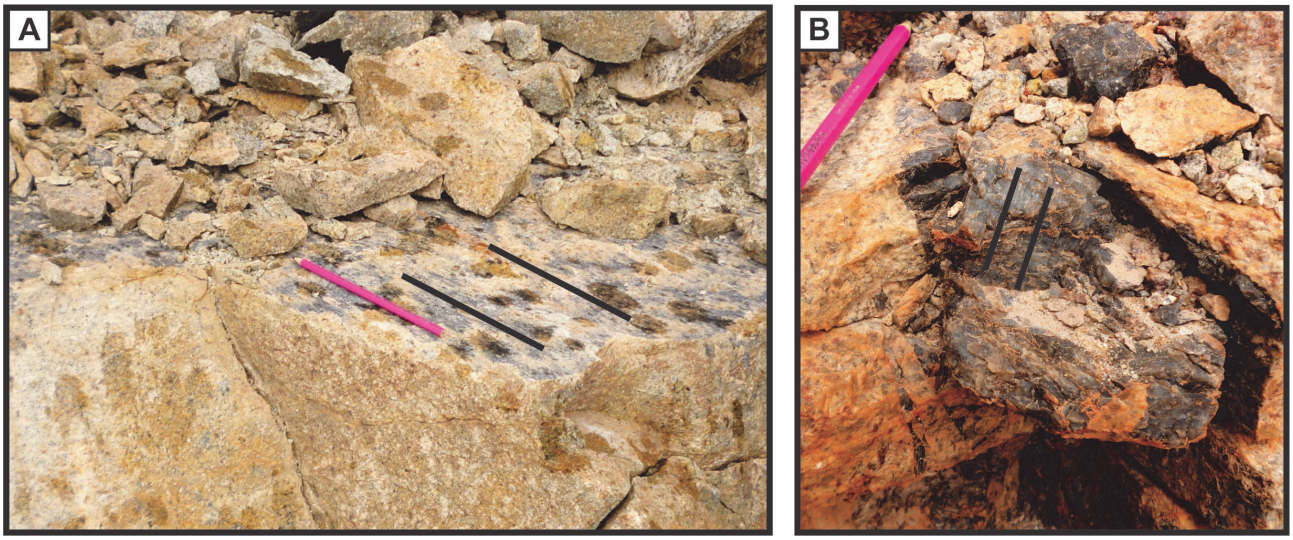

Figure 9. Less commons structures. A) Very low angle reverse fault plane filled with riebeckite. Slickenlines indicate transport to WNW (pencil tip); B) Hybrid fracture filled with fibrous cryolite.
Figura 9. Estruturas menos comuns. A) Plano de falha inversa de muito baixo ângulo preenchido com riebeckita. Estrias indicam transporte para WNW (ponta do lápis); B) Fratura híbrida preenchida com criolita fibrosa.

crystals. The wall zone consists predominantly of albite and quartz crystals, with hipidiomorphic texture. The intermediate zone is marked by the preferential orientation of the minerals perpendicular to the wall and abrupt increase of the size of the minerals. The nucleus is usually formed only by cryolite.

There are two types of pegmatite veins visible in the whole mine front, from level 210 to 140 (levels are indicated in Fig. 4). The prevalent type is that of metric tabular bodies, with no more than 1 meter thick, emplaced in horizontal extension fractures (Fig. 11B). The other group is formed by tabular bodies emplaced in the reverse fault planes (Fig. 11C). These veins have centimeter to decimeter thickness and can be discontinuous in a same fault plane. Both types of pegmatite veins are formed by quartz, albite, riebeckite, K-feldspar and polylithionite and, to a lesser extent, cryolite, fluorite, xenotime-(Y), thorite and genthelvite. Locally dykes of aplite cut the pegmatite veins (Fig. 11D).

The horizontal pegmatite bodies (Fig. 12) have a thin, well-marked, border (centimeter), with minerals sizes ranging from 0.1 to 5 cm. From the border to the center of the bodies there is a systematic increase in the size of the minerals, without, however, defining a zoning. The interior of the bodies is homogeneous, with anhedral to subhedral minerals generally around 5 cm in size.

In the subvertical pegmatite bodies the internal zoning is also not well defined, except for the border zone, which is also thin. The minerals in the border zone are smaller than the minerals in the interior.

The orientation of the planar pegmatite bodies (horizontal or subvertical) is controlled by the contractional structures in the CAG.

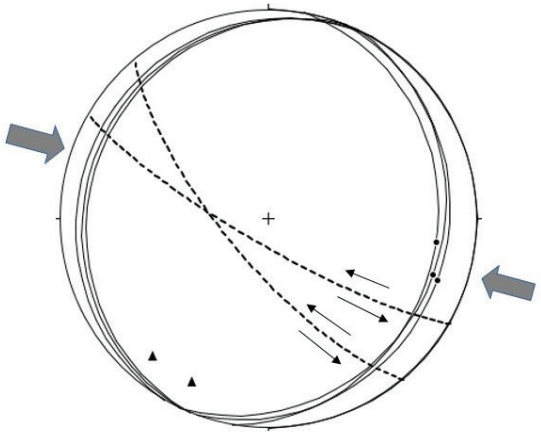

Figure 10. Planes of low angle reverse faults (great circles) with riebeckite slickenlines (dots), hybrid fractures (doted lines) with fibers of cryolite (triangles) and approximate orientation of the σ1 (arrows) (N: 13). Equal-area (Schmidt-Lambert) stereographic projection, lower hemisphere.
Figura 10. Planos de falhas inversas de baixo ângulo (grandes círculos) com estrias de riebeckita (pontos), fraturas hibridas (linhas tracejadas) com fibras de criolita (triângulos) e orientação aproximada do σ1 (flechas) (N: 13). Projeção estereográfica equiárea (Schmidt-Lambert) hemisfério inferior.

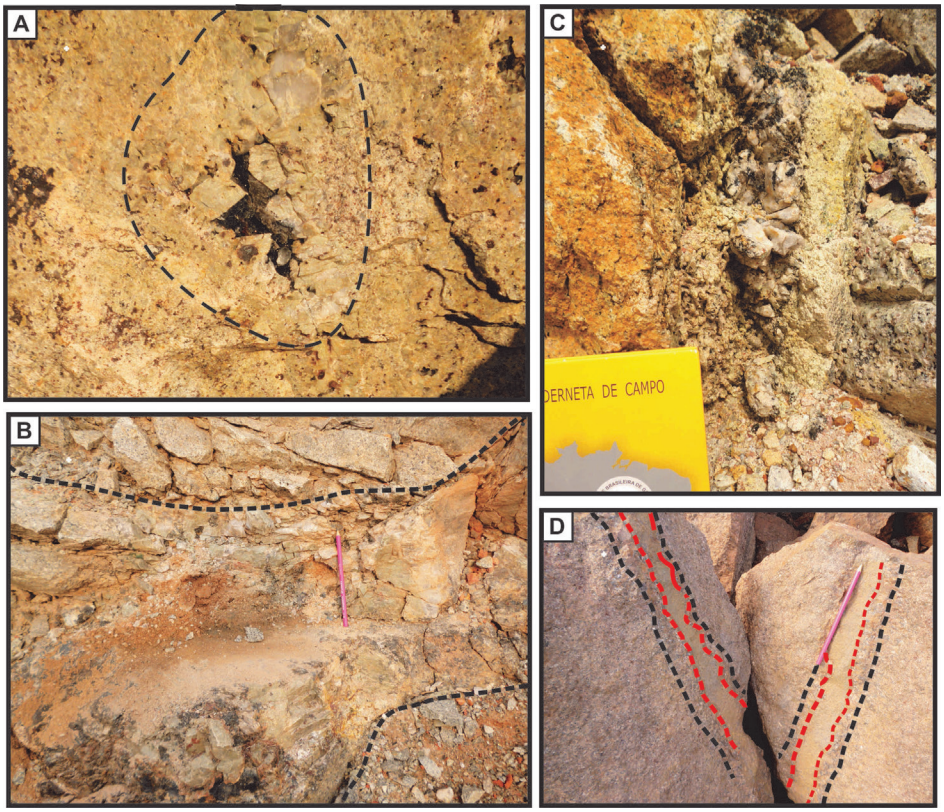

Figure 11. Occurrence forms of pegmatites. A) Pegmatite in miarolitic cavity (photo width: 50 cm); B) Pegmatite body emplaced in horizontal extension fracture; C) Pegmatite body emplaced in reverse fault plane; D) Aplite dike (dotted red line) cutting a pegmatite vein (dotted black line).
Figura 11. Formas de ocorrência de pegmatitos. A) Pegmatito em cavidade miarolítica (largura da foto: 50 cm); B) Corpo de pegmatito alojado em fratura extensional horizontal; C) Corpo de pegmatito alojado em plano de falha inversa; D) Dique de aplito (linha tracejada vermelha) cortando veio de pegmatito (linha tracejada preta).

Figure 12. Pegmatite body emplaced in horizontal extension fracture (black line) associate with reverse fault plane (dotted black lines).
Figura 12. Corpo de pegmatito alojado em fratura extensional horizontal (linha preta) associado a plano de falha inversa (linhas pretas tracejadas).

The subvertical pegmatite veins are emplaced in planes of reverse faults and the horizontal pegmatites veins are housed in extension fractures. The horizontal pegmatite bodies are perpendicular to the minimum stress axis (σ3) and the subvertical pegmatite veins occur in the reverse fault planes positioned at approximately 60º from σ3 (Fig. 8B). Pegmatite veins are preferably emplaced in fault planes that dip to SW. Horizontal and subvertical planes are physically connected and the textural characteristics of the pegmatites in these places suggest that the fault planes worked as fluid conducts to form the horizontal veins. The minerals in the pegmatites do not present evidences of deformation when analyzed under the optical microscope.

4 Discussion

The pegmatite bodies hosted in the CAG have a common geometric arrangement and share a same mineralogy, indicating that they all originate from the same source and thus they correspond to a pegmatite group (London, 2015). Based on the characteristics of the structural setting, mineralogy, composition and texture, they are classified as granitic type of the REL (rare elements) class and as NYF (Nb, Y and REE, and F) family (Cerny & Ercit,2005) and as F-REE-Li vein-type granite pegmatite (Dill, 2015). Although evolved pegmatites can originate dykes at great distance, which propagate vertically to upper crust from a pluton placed in the lower/middle crust, this does not appear to be the case of the studied pegmatites. The fact that they have the same mineralogical composition of the host rock strongly suggests that their emplacement occurred in the parental rock itself.

With reduced surface dimensions (2 km x 1.5 km), probably the CAG cooled fast and this can be considered a constraint to generate pegmatite dykes. However, another factor may have been decisive for the generation of pegmatites. In the case of plutons located in the cold upper crust, magmas with low *solidus* temperature (relatively evolved) can form pegmatites (Baker, 1998), and the *solidus* temperature of the CAG is estimated to be about 500ºC (Costi *et al*., 2009).

The existence of reverse fault planes and extension fractures with and without pegmatite indicates that the fluid pressure of the pegmatite did not originate the system of fractures established in the host rock (CAG). The absence of deformation in the minerals that compose the pegmatite indicates that the emplacement of the pegmatite is subsequent to the formation of the contractional system. That is, before the pegmatites emplacement, the CAG, already fully crystallized, was subjected to a tectonic load and then had a brittle behavior. Effectively, the CAG crystallized under P-T conditions of 1 kbar and 650 ºC, to a depth < 1 km (Lenharo, 2003). At this crustal level, ductile behavior would not be expected, unless the CAG was syntectonic. When the pegmatites intrusion occurred, the CAG was positioned above the critical crustal depth (Brisbin, 1986), where minimum normal stress is vertical. This explains why reverse fault planes were not preferred sites for the pegmatite emplacement. With the minimum normal-stress vertical, the horizontal extension fractures were the preferential sites for the pegmatites. The reverse fault planes, where the pegmatite veins are poorly developed, were mainly conduits for F-enriched low viscosity residual melt that rise from deeper parts of CAG and were housed in the fractures perpendicular to the minimum stress axis. The existence of more tabular bodies in the SW than in the NE dip fault planes should be linked to particular conditions of normal stress and fluid pressure.

Pegmatites of the REL class are characteristic of intermediate to shallow crustal levels. In this environment, the host rock exhibits brittle behavior, like the structures present at Pitinga mine. On the other hand, the pegmatites of the NYF family have tectonic affiliation with anorogenic granites (Cerny *et al*., 2012), as is the case of the CAG.

The previous works dealing with the emplacement of the AEG mention the influence of a shear zone striking NE-SW, left lateral (Bastos Neto *et al*., 2014) or right lateral (Siachoque *et al*., 2017), or the influence of N-S structures (Costi *et al*., 2000; Minuzzi *et al*., 2006). However, the structures described above - slickenlines that point down deep, horizontal tensile fractures - and the determinated horizontal intermediate

(σ2) stress are convincing evidence that the origin of the contractional structures is not linked to a transpressional regime. The N320 trend of the fault planes highlighted in the Pitinga mine is regionally penetrative. This trend is quite clear in lineaments in SRTM images of the Madeira Granite area and predominates in the aeromagnetic anomalies of this portion of the Central Amazonian Province (Rosa *et al*., 2014). The Pitinga mine is located on the border of the Central Amazonian Province, but at only 50 km from the limit with the Ventuari-Tapajós Province. The contractional deformation of the CAG may follow from the final efforts generated during the amalgamation of juvenile terrains (2.0 - 1.8 Ga) which resulted in the formation of the Ventuari-Tapajós Province. The Ventuari-Tapajós collisional orogenic belt comprised the subduction (~1.89Ga) of an oceanic plate under the Central Amazonian Province (Valério *et al*., 2006, Rosa *et al*., 2014). The vergence to NE of the contractional structures of the CAG (imbricated zones, horses) is consistent with the expected orientation of the foreland structures in the Ventuari-Tapajós orogen.

Exist many examples of pegmatite hosted in A-type peralkaline granites of crustal shallow level. In these cases, the fluid pressure generates the fractures in the final stages of the magmatic evolution (hydraulic fracturing). The data present in this paper suggest the existence of tectonic fractures in the host rock when the emplacement of the pegmatites occurred at the studied structural level. Examples of previous development of space into which pegmatite may be emplaced also exist. One example is the REE pegmatite of the Strange Lake Complex (Canada). This complex is a small anorogenic granite with sub circular shape (~1189 Ma; Pillet *et al*., 1989). Just as it occurs in the CAG, the pegmatites are hosted in the youngest phase of the complex. The pegmatite occurs as a large lens and many thin subvertical dikes (Miller, 1990). The emplacement of the granite created fractures in the roof zone, then the pegmatite emplaced in these previous developed sites. Another example of REE pegmatite, but associated to a granitic gneiss host, is the Kipawa syenite Complex (~1240 Ma) in Canada. The complex is strongly metamorphosed and underwent three deformation stages. The pegmatites are undeformed small folded veins. They are hosted in the cleavage planes of the F1 folds that are folded in the F2 stage (Currie & Breemen, 1996). Therefore, the emplacement of the pegmatite is posterior to the development of these planes.

5 Conclusion

All the pegmatites associated to the albite-enriched granite (~1.83 Ga) are classified as F-REE-Li vein–type granite pegmatite. The pegmatite bodies hosted in the albite-enriched granite have a common geometric arrangement (horizontal bodies and subvertical veins) and share a same mineralogy, which is characterized by riebeckite, polylithionite, albite, quartz and cryolite with minor genthelvite, xenotime-(Y) and fluocerite-(Ce). They all originate from the same source. They have the same mineralogical composition of the albite-enriched granite. They occur exclusively in this rock. These characteristics indicate that their emplacement occurred in the parental rock itself.

With reduced surface dimensions (2 x 1.5 km), the albite-enriched granite cooled fast. However, its location in the cold upper crust and the low *solidus* temperature allowed pegmatites formation. The structural features of pegmatites and host rock show that at the structural level of the studied pegmatites the albite-enriched granite was crystallized when these veins positioned.

The geometric arrangement of the pegmatites is settled by contractional brittle structures (reverse faults ~N320/60SW, imbrication fans and horses) in the albite-enriched granite. When the pegmatites intrusion occurred, the albite-enriched granite was positioned above the critical crustal depth, where minimum normal stress is vertical. The well-marked geometric arrangement of the structures indicates that they are tectonic; and the existence of reverse fault planes and extension fractures with and without pegmatite show that the fractures that host the pegmatites were not formed by the fluid pressure.

As the CAG was positioned above the critical crustal depth, the reverse fault planes were not the preferred sites for the pegmatite emplacement,

but the horizontal extension fractures associated to these planes. These reverse fault planes were essentially the conduits for the fluid.

The brittle structures in the CAG probably were formed by the final efforts of the amalgamation of juvenile terrains of which the Ventuari-Tapajós Province results. The vergence to NE of the contractional structures of the CAG is consistent with the expected orientation of the foreland structures in the Ventuari-Tapajós orogeny.

Acknowledgments. The authors wish to thank two anonymous reviewers and the editor for their suggestions and critical comments, which significantly contributed to improve the manuscript. The realization of this work would not have been possible without the support given by the Mineração Taboca Ltda., through Guilherme Vanzela and team. The Conselho Nacional de Desenvolvimento Científico e Tecnológico (CNPq) is acknowledged for financial support (Project 405839/2013-8).

References

Baker, D.R. 1998. The escape of pegmatite diker from granitic plutons: constraints from new models of viscosity and dike propagation. *The Canadian Mineralogist*, 36: 255-263.

Bastos Neto, A.C., Pereira, V.P., Lima, E.F., Ferron, J.M.T.M., Minuzzi, O.R.R., Prado, M., Ronchi, L.H., Frantz, J.C. & Botelho, N.F. 2005. O depósito de criolita da mina Pitinga (Amazonas). *In*: Marini, J.O., Queiroz, E., Ramos, B.W. (Ed.). *Caracterização de Depósitos Minerais em Distritos Mineiros da Amazônia*. DNPM/CTMINERAL/ADIMB, Brasília, p. 477–552.

Bastos Neto, A.C., Pereira, V.P., Ronchi, L.H., Lima, E. F. & Frantz, J.C. 2009. The world-class Sn, Nb, Ta, F (Y, Ree, Li) deposit and the massive cryolite associated with the albite-enriched facies of the Madeira A-type granite, Pitinga Mining District, Amazonas State, Brazil. *The Canadian Mineralogist*, 47: 1329-1357.

Bastos Neto, A.C., Ferron, J.T.M.M., Chauvet, A., Chemale Jr, F., Lima, E.F.L., Barbanson, L. & Costa, C.F.M. 2014. U–Pb dating of the Madeira Suite and structural control of the AEG at Pitinga (Amazonia, Brazil): Evolution of the A-type magmatism and implications for the genesis of the MadeiraSn–Ta–Nb (REE, cryolite) world-class deposit. *Precambrian Research*, 243: 181-196.

Bons, P.D., Elburg, M.A. & Gomez-Rivas, E. 2012. A review of the formation of tectonic veins and their microstructures. *Journal of Structural Geology*, 43: 33-62.

Boyer, S.E. & Elliott, D. 1982. Thrust systems. *The American Association of Petroleum Geologists Bulletin*, 66(9): 1196-1230.

Brisbin, W.C. 1986. Mechanics of pegmatite intrusion. *American Mineralogist*, 71: 644-651.

Cerny, P. & Ercit, T. S. 2005. The classification of granitic pegmatites revisited. *The Canadian Mineralogist*, 43: 2005-2026.

Cerny, P., London, D. & Novák, M. 2012. Granitic pegmatites as reflections of their sources. *Elements*, 8: 289-294.

Costi, H.T. 2000. *Petrology of rare metals-, high-F-alkaline granites: The example of the albite granite from the Pitinga Mine, Amazonas State, Brazil*. Belém, 345p. Doctoral thesis, Institute of Geosciences, Federal University of Pará.

Costi, H.T., Dall'Agnol, R. & Moura, C.A.V. 2000. Geology and Pb–Pb geochronology of Paleoproterozoic volcanic and granitic rocks of the Pitinga Province, Amazonian craton, northern Brazil. *International Geology Review*, 42: 832-849.

Costi, H.T., Dall'Agnol, R., Pichavant, M. & Ramo, O.T. 2009. The peralkaline tin-mineralized Madeira cryolite albite-rich granite of Pitinga, Amazonian Craton, Brazil: Petrography, mineralogy e crystallization processes. *The Canadian Mineralogist*, 47: 1301-1327.

Currie, K.L. & Breemen, O.V. 1996. The origin of rare minerals in the Kipawa syenite Complex, western Quebec. *The Canadian Mineralogist*, 34: 435-451.

Dill, H.G. 2015. Pegmatites and aplites: Their genetic and applied ore geology. *Ore Geology Reviews,* 69: 417-561.

Dill, H.G. 2016. The CMS classification scheme (Chemical composition-Mineral assemblage-Structural geology) – linking geology to mineralogy of pegmatitic and aplitic rocks.

Neues Jahrbuch fr Mineralogie Abhandlungen, 193: 231-264.

Dill, H.G. 2018. Geology and chemistry of Variscan-type pegmatite systems (SE Germany) – With special reference to structural and chemical pattern recognition of felsic mobile components in the crust. *Ore Geology Reviews*, 92: 205-239,

Ferron, J.M.T.M., Bastos Neto, A.C., Lima, E.F., Costi, H.T., Moura, C., Prado, M. & Galarza, M. 2006. Geologia e geocronologia Pb–Pb de rochas graníticas e vulcânicas ácidas a intermediárias Paleoproterozóicas da Província Pitinga, Cráton Amazônico. *Revista Brasileira de Geociências*, 36(3): 499–512.

Gibbs, A.K. & Barron, C.N. 1983. The Guiana Shield reviewed. *Episodes*, 2: 7-14.

Lenharo, S.L. 1998. *Evolução magmática e modelo metalogenético dos granitos mineralizados da região de Pitinga, Amazonas, Brasil*. São Paulo, 290p. Doctoral thesis, Escola Politécnica, Universidade de São Paulo.

Lenharo, S.L.R., Pollard, P.J. & Born, H. 2003. Petrology and textural evolution of granites associated with tin and rare-metals mineralization at the Pitinga mine, Amazonas, Brasil. *Lithos*, 66: 37-61.

London, D. 2015. Reading pegmatites: Part 1 – What beryl says. *Rocks and Minerals*, 90: 138-149.

Miller, R.R. 1990. The Strange Lake pegmatite-aplite hosted rare metal deposit, Labrador. *Current Research*, Newfoundland Departament of Mines and Energy, Geological Survey Branch, Report 90(1): 171-182.

Minuzzi, O.R.R., Bastos Neto, A.C., Flores, J.A.A., Pereira, V.P. & Ferron, J.T.M.M. 2006. O depósito criolítico maciço e o minério disseminado de criolita da mina Pitinga (Amazonas, Brasil). *Revista Brasileira de Geociências*, 36(Supl.): 104–123.

Pillet, D., Bonhomme, M.G., Duthou, J.L. & Chenevoy, M. 1989. Chronologie Rb/Sr et K/Ar du granite peralkalin du lac Brisson, Labrador central, Noveau-Quebec. *Canadian Journal of Earth Sciences*, 26: 328- 332.

Pires, A.C. 2010. *Xenotima, gagarinita, fluocerita e waimirita da mina de Pitinga (AM): mineralogia e avaliação preliminar do potencial do albita granito para exploração de elementos terras raras e ítrio*. Porto Alegre, 199p. Doctoral thesis, Institute of Geosciences, Federal University of Rio Grande do Sul.

Rosa, J.W.C., Rosa, J.W.C. & Fuck, R.A. 2014. Geophysical structures and tectonic evolution of the southern Guyana shield, Brazil. *Journal of South American Earth Sciences*, 52: 57-71.

Siachoque, A., Salazar, C.A. & Trindade, R. 2017. Emplacement and deformation of A-type granite (Amazonian Craton, Brazil). *Lithos*, 277: 284-301.

Stolnik, D. 2015. *Caracterização da xenotima na fácies pegmatítica do albita granito de núcleo, Pitinga (AM)*. Porto Alegre, 67p. Course conclusion monograph, Geology course, Institute of Geosciences, Federal University of Rio Grande do Sul.

Valério, C.S., Souza, V.S., Macambira, M.J.B. & Galarza, M.A. 2006. Geoquímica e geocronologia Pb-Pb em zircão da Suíte Intrusiva Água Branca, município de Presidente Figueiredo (AM): evidências de colisão no Paleoproterozoico da Amazônia Ocidental. *Revista Brasileira de Geociências*, 36(2): 359-370.

Tassinari, C.C.G. & Macambira, J.B.M. 1999. Geochronological provinces of the Amazonian Craton. *Episodes*, 22: 174-182.

Manuscrito 734 | Recebido em nov. de 2017 | Aceito em dez. de 2018 | Editor: Lauro V. S. Nardi